


RESEARCH

Open Access



Mesenchymal stromal cell therapy reduces lung inflammation and vascular remodeling and improves hemodynamics in experimental pulmonary arterial hypertension

Lucas de Mendonça^{1,2†}, Nathane S. Felix^{1,2†}, Natália G. Blanco^{1,2}, Jaqueline S. Da Silva³, Tatiana P. Ferreira⁵, Soraia C. Abreu^{1,2}, Fernanda F. Cruz^{1,2}, Nazareth Rocha^{1,4}, Patrícia M. Silva⁵, Vanessa Martins^{1,6}, Vera L. Capelozzi⁶, Gizele Zapata-Sudo³, Patricia R. M. Rocco^{1,2} and Pedro L. Silva^{1,2*} 

Abstract

Background: Experimental research has reported beneficial effects of mesenchymal stromal cell (MSC) therapy in pulmonary arterial hypertension (PAH). However, these studies either were based on prophylactic protocols or assessed basic remodeling features without evaluating possible mechanisms. We analyzed the effects of MSC therapy on lung vascular remodeling and hemodynamics and its possible mechanisms of action in monocrotaline (MCT)-induced PAH.

Methods: Twenty-eight Wistar rats were randomly divided into two groups. In the PAH group, animals received MCT 60 mg/kg intraperitoneally, while a control group received saline (SAL) instead. On day 14, both groups were further randomized to receive 10^5 adipose-derived MSCs or SAL intravenously ($n = 7$ /group). On day 28, right ventricular systolic pressure (RVSP) and the gene expression of mediators associated with apoptosis, inflammation, fibrosis, Smad-1 levels, cell proliferation, and endothelial–mesenchymal transition were determined. In addition, lung histology (smooth muscle cell proliferation and plexiform-like injuries), CD68⁺ and CD163⁺ macrophages, and plasma levels of vascular endothelial growth factor (VEGF) and platelet-derived growth factor (PDGF) were evaluated.

Results: In the PAH group, adipose-derived MSCs, compared to SAL, reduced mean RVSP (29 ± 1 vs 39 ± 2 mmHg, $p < 0.001$), lung tissue collagen fiber content, smooth muscle cell proliferation, CD68⁺ macrophages, interleukin-6 expression, and the antiapoptotic mediators Bcl-2 and survivin. Conversely, expression of the proapoptotic mediator procaspase-3 and plasma VEGF increased, with no changes in PDGF. In the pulmonary artery, MSCs dampened the endothelial–mesenchymal transition.

(Continued on next page)

* Correspondence: pedro.leme@gmail.com

†Equal contributors

¹Laboratory of Pulmonary Investigation, Carlos Chagas Filho Biophysics Institute, Federal University of Rio de Janeiro, Centro de Ciências da Saúde, Avenida Carlos Chagas Filho, s/n, Bloco G-014, Ilha do Fundão, Rio de Janeiro, RJ 21941-902, Brazil

²National Institute of Science and Technology for Regenerative Medicine, Rio de Janeiro, RJ, Brazil

Full list of author information is available at the end of the article



(Continued from previous page)

Conclusion: In MCT-induced PAH, MSC therapy reduced lung vascular remodeling, thus improving hemodynamics. These beneficial effects were associated with increased levels of proapoptotic markers, mesenchymal-to-endothelial transition, reduced cell proliferation markers, and inflammation due to a shift away from the M1 phenotype.

Keywords: Pulmonary arterial hypertension, Mesenchymal stromal cells, Hemodynamics, Lung vascular remodeling, Macrophage phenotype

Background

Pulmonary arterial hypertension (PAH) is a progressive disease, caused by a variety of pulmonary or cardiac disorders, which carries high rates of morbidity and mortality. PAH is characterized by a progressive increase in pulmonary arterial pressure, right heart dysfunction, and vascular remodeling, which leads to right ventricular failure [1–3]. Specific features of the vascular remodeling seen in PAH include apoptosis and proliferation of pulmonary vascular endothelial cells, muscularization of distal pulmonary arterioles, deposition of extracellular matrix proteins, and perivascular inflammation [2].

Several clinical [1, 4] and experimental [5–9] studies have sought to investigate the pathophysiology of PAH, which remains controversial [10]. Its characteristic perivascular inflammation involves interplay among several cell types, which include T and B lymphocytes, dendritic cells, mast cells, and macrophages. It is worth noting that perivascular macrophages—particularly the M1 phenotype—represent one of the main sources of IL-6 [11]. Although a heightened inflammatory state is clearly associated with PAH [2], the contribution of macrophage phenotypes to PAH pathophysiology remains unclear. Besides the role of inflammation, specific growth factors with proangiogenic effects may contribute to endothelial cell proliferation and fibroblast activation, which, in turn, contribute toward lung vascular remodeling [8, 10, 12].

The only currently available pharmacological therapies for PAH focus on vasodilatory effects, decreasing RV afterload, and relieving symptoms [13]. To date, no therapy has been able to minimize inflammation and vascular remodeling processes and thus modify the natural history of the disease.

Stem cell therapy may constitute a new treatment modality for PAH [14, 15]. Particularly, mesenchymal stromal cells (MSCs) may have the ability to secrete paracrine factors which can mitigate tissue damage [16]. Preclinical studies using MSCs in animals with PAH reported reduction in inflammation [16] and remodeling [17–20], which may be associated with improvement in hemodynamics [19]. However, those studies evaluated lung vascular remodeling based on either RV ratios [18, 19] or basic wall thickness [17, 20], instead of fulfilling histological criteria for PAH [21]. Furthermore, there is very little information about the cellular mechanisms (which includes macrophage

subpopulations) and molecular factors [22] responsible for the beneficial effects of MSCs on right-heart hemodynamics in PAH.

The present study uses a rat model of monocrotaline-induced PAH to investigate the effects of MSC therapy on vascular histology and hemodynamics and to attempt to elucidate the possible mechanisms of MSC action in PAH, through analyses of macrophage subpopulations, expression of growth factors, levels of proapoptotic and antiapoptotic mediators, endothelial–mesenchymal transition, and cell proliferation.

Methods

This study was approved by the Institutional Animal Care and Use Committee of the Health Sciences Centre, Federal University of Rio de Janeiro (CEUA 114/14), and registered with the Brazilian National Council for Animal Experimentation Control. All animals received humane care in compliance with the “Principles of Laboratory Animal Care” formulated by the National Society for Medical Research and the US National Academy of Sciences *Guide for the Care and Use of Laboratory Animals*. The present study followed the ARRIVE guidelines for reporting of animal research [23].

Animal preparation and experimental protocol

On day 0, echocardiography analysis of the right ventricle was performed in 28 male Wistar rats (weight 235 ± 21 g), which were then randomized into two groups: monocrotaline-induced PAH (MCT, $n = 14$), in which animals received 60 mg/kg of MCT intraperitoneally (i.p.) (C2401; Sigma Chemical Co., St Louis, MO, USA); and control (CTRL, $n = 14$), in which animals received a similar volume of saline solution i.p. On day 14, cardiovascular function impairment was assessed by repeat echocardiography in the CTRL and MCT groups. Both groups were randomized again to receive either MSCs ($n = 7$, 10^5 cells intravenously (i.v.) through the jugular vein diluted in 50 μ l saline solution) or an equivalent volume of saline solution (SAL, $n = 7$). On day 28, echocardiography was repeated, hemodynamic parameters were measured, and animals were killed for postmortem analyses.

Adipose cell culture

For isolation of adipose-derived MSCs, male Wistar rats were killed with sevoflurane (Sevorane® 2.0 vol.%; Cristália, Itapira, São Paulo, SP, Brazil) and the inferior vena cava was transected. Fat tissue around the epididymis was identified, removed, and placed in 1× phosphate-buffered saline (PBS). The tissue was then mechanically dissociated and placed in 2 ml of type 1 collagenase solution (1 mg/ml) for 35 minutes at 37 °C, with homogenization every 10 minutes. DMEM (Invitrogen Life Technologies, Grand Isle, NY, USA) supplemented with 10% fetal bovine serum (FBS; Hyclone, Rockford, IL, USA), 1% penicillin/streptomycin (Pen/Strep; Invitrogen Life Technologies), and 2 mM L-glutamine (Invitrogen) was added to the solution for collagenase inactivation, and the whole solution was centrifuged at 300 × g for 5 minutes. The pellet was transferred into tissue culture dishes containing the same medium. The culture medium was changed on the day after extraction and three times a week thereafter. MSCs were expanded in culture using Iscove's Modification of Dulbecco's Medium (IMDM; Hyclone), supplemented with 10% FBS, 10% horse serum (Hyclone), 1% Pen/Strep, and 2 mM L-glutamine; MSCs were used at the third to sixth passage. They were kept in culture at confluence no greater than 70%. Immediately before injections, cells were lifted using 2.5% Trypsin/EDTA (Invitrogen Life Technologies). Cell density and viability was determined using Trypan blue staining and counted using a hemocytometer. Cell pellets were then resuspended in 1× PBS to a final concentration of 1 × 10⁵ cells per 50 µl immediately prior to injection.

Approximately 1 × 10⁵ cells at the third passage were characterized as MSCs according to the International Society of Cellular Therapy Consensus; that is, adhesion to plastic under standard conditions, expression of specific surface markers (CD73, CD90, and CD105) and lack of others (CD11b, CD19, CD34, CD45), and ability to differentiate into mesenchymal lineages (such as adipocytes, chondrocytes, and osteoblasts) under in-vitro conditions [24]. For flow cytometry analysis, we used antibodies against CD90-PE (thymocytes), CD34-PE (hematopoietic precursors), and CD29-FITC (nonhematopoietic precursors) (BD Biosciences, USA). The absence of CD90 and CD34 and the presence of CD29 were used to identify MSCs [25]. The different MSC populations were further characterized by their capacity to differentiate into osteoblasts and chondroblasts. Osteogenic differentiation was induced by culturing MSCs for up to 3 weeks in DMEM 10% FBS and 15 mM HEPES (Sigma Chemical Co., St Louis, MO, USA), supplemented with 10⁻⁸ M/L dexamethasone (Sigma Chemical Co.), 5 µg/ml ascorbic acid 2-phosphate (Sigma Chemical Co.), and 10 mM/L β-glycerolphosphate (Sigma Chemical Co.). To observe calcium deposition, cultures were stained with Alizarin

Red S (Nuclear, SP, Brazil). To induce chondrogenic differentiation, MSCs were cultured in DMEM supplemented with 10 ng/ml TGF-β1 (Sigma, St. Louis, MO, USA), 50 nM ascorbic acid 2-phosphate (Sigma Chemical Co.), and 6.25 mg/ml insulin for 3 weeks. To confirm differentiation, cells were fixed with 4% paraformaldehyde in PBS for 1 hour at room temperature, and then stained with Alcian Blue (pH 2.5) [26].

Echocardiography

For echocardiographic assessment of cardiovascular function, rats were anesthetized with sevoflurane (Sevorane® 2.0 vol.%; Cristália), shaved over the precordial region, and examined with a Vevo 770 system (VisualSonics, Toronto, ON, Canada) coupled to a 30-MHz transducer. Images were obtained from parasternal views. Pulsed-wave Doppler was used to measure the pulmonary artery acceleration time (PAT) and pulmonary artery ejection time (PET), and the PAT/PET ratio was used as an indirect index of PAH. All parameters followed the American Society of Echocardiography and European Association of Cardiovascular Imaging guidelines, as validated in a previous article on noninvasive assessment of murine pulmonary arterial pressure [27, 28].

Hemodynamic measurements

Rats were anesthetized with fentanyl 100 µg/kg i.p. (União Química, São Paulo, SP, Brazil) and midazolam 5 mg/kg i.p. (Dormicum, União Química, São Paulo, SP, Brazil). If required, additional anesthesia was provided by inhaled sevoflurane through a nasal device. Animals were placed in dorsal recumbency and the skin and muscle tissue of the anterior chest wall were removed until the ribs were visible. The thorax was then opened and a heparinized 19-G winged infusion set (Embramac, Itapira, SP, Brazil) was inserted into the RV. The RV systolic pressure (RVSP) and RV contraction rate (RV dp/dtmax) were assessed with a physiological data acquisition system (LabChart 7.0; ADInstruments, Sydney, Australia). Blood samples were collected through inferior vena cava puncture into a heparinized syringe. These samples were then centrifuged at 1500 × g for 5 minutes at 4 °C for plasma retrieval for enzyme-linked immunosorbent assay (see later). At the end of the experiment, animals were euthanized by i.v. injection of sodium thiopental 25 mg (Cristália) followed by complete exsanguination through transection of the abdominal aorta.

Determination of pulmonary artery function

After hemodynamic measurements, the heart and lung were removed. The main pulmonary artery was carefully dissected and cleaned of connective tissue. Arteries were attached to a force transducer and placed in vertical chambers filled with modified Tyrode's

solution (123 mM NaCl, 4.7 mM KCl, 1.2 mM MgCl₂, 1.2 mM KH₂PO₄, 15.5 mM NaHCO₃, 1.2 mM CaCl₂, and 11.5 mM dextrose), which were oxygenated and kept at 37 °C. After a stabilization period of 2 hours in 1.5 g tension, the solutions were exposed to increasing doses of phenylephrine (Phe, 1 nM–10 μM). After the contraction plateau, the arteries were exposed to increasing doses of acetylcholine (ACh, 1 nM–10 μM) to evaluate endothelial function by the maximum relaxation capacity.

Quantification of lung collagen

The right upper lobe of the lung was homogenized in Tris–HCl 0.05 M and NaCl 1 M containing protease inhibitor (Hoffmann-La Roche) (pH 7.4). Total soluble collagen was extracted overnight at room temperature and quantified using the Sircol™ kit (Bicolor, Newton Abbey, UK). The results were expressed as micrograms of collagen/milligram of total protein by Bradford's technique.

Optical microscopy

For optical microscopy (OM) analysis, an additional 24 Wistar rats ($n = 6$ /group) were subjected to the same protocol as already described. To keep lungs inflated before fixation, a similar end-expiratory pressure (3 cmH₂O) was achieved among all groups by a brief period of mechanical ventilation (Flexivent; SCIREQ, Canada). Heparin (1000 IU) was injected into the tail vein to allow better visualization of lung structures under OM. To extract the lungs, a laparotomy was performed and the inferior vena cava transected to kill the animals by exsanguination. The left lung was then quickly isolated, frozen in liquid nitrogen, and placed in Carnoy's solution. The lungs were dehydrated in a graded ethanol series and embedded in paraffin. Slices (4-μm thick) were cut, deparaffinized, and stained with hematoxylin–eosin (H&E). The histopathological features of the pre-acinar and intra-acinar pulmonary arteries were classified according to Pietra et al. [21] on the basis of: medial hypertrophy with increase in cross-sectional area; intimal thickening, defined as concentric laminar, eccentric, or concentric nonlaminar (both lesion types composed of fibroblasts and connective tissue matrix); and dilatation lesions. These histopathological features were graded on a five-point, semiquantitative, severity-based scoring system as follows: 0 = normal, 1 = changes in 1–25% of examined tissue, 2 = changes in 26–50% of examined tissue, 3 = changes in 51–75% of examined tissue, and 4 = changes in 76–100% of examined tissue. This semiquantitative five-point score has been validated in different animal models [26, 29]. Scoring was assessed independently by one coauthor (VLC), who is an expert in lung pathology and was blinded to group allocation.

Lung slices were also stained with the modified Russel–Movat method to highlight the muscular, connective, and elastic fibers of lung vessels in histological slides [30]. In brief, a mixture of five stains—Alcian Blue, Verhoeff hematoxylin, and Crocein Scarlet combined with acidic fuchsin and saffron—was used. At pH 2.5, Alcian Blue was fixed by electrostatic binding with the acidic mucopolysaccharides. Verhoeff hematoxylin has a high affinity for nuclei and elastin fibers, which are negatively charged. The combination of Crocein Scarlet with acidic fuchsin stains acidophilic tissue components in red. Then collagen and reticulin fibers were unstained by a reaction with phosphotungstic acid, and stained yellow by saffron. Smooth muscle hypertrophy and vascular endothelial growth factor (VEGF) expression were quantified using a weighted scoring system, as described elsewhere [31, 32]. Briefly, values from 0 to 4 were used to represent the severity of smooth muscle hypertrophy and VEGF expression, with 0 standing for no effect and 4 for maximum severity. Additionally, the extent of smooth muscle hypertrophy and VEGF expression per field of view was determined using values of 0–4, with 0 standing for no appearance and 4 for complete involvement. The final score for each feature was calculated as the product of extension and severity, ranging from 0 to 16. Scoring was assessed independently by one coauthor (VLC), who is an expert in lung pathology and was blinded to group allocation.

Transmission electron microscopy of pulmonary arteries

Three slices measuring 2 mm × 2 mm × 2 mm were cut from three different segments of the right inferior lung. They were then fixed in 2.5% glutaraldehyde and phosphate buffer, 0.1 M (pH 7.4), for transmission electron microscopy (TEM) analysis (JEOL 1010 Transmission Electron Microscope; Japan Electron Optics Laboratory Co, Tokyo, Japan). For each TEM image (20 per animal), an injury score was determined. The following parameters were analyzed, considering the pulmonary arteries: medial hypertrophy and concentric laminar intimal thickening in the pre-acinar artery; and basement membrane thickening, myofibroblast proliferation, endothelial hyperplasia, and smooth muscle fibers in the intra-acinar artery. These parameters were graded on a five-point scoring system similar to that already described for histopathological features.

Macrophage immunohistochemistry

Sections were deparaffinized and hydrated and the slides were incubated with 10 mM sodium citrate. Endogenous peroxidase activity was blocked with 3% hydrogen peroxide. Slides were washed in TBS with 0.05% Tween-20 (Sigma), blocked with serum-free protein block (Dako, Carpinteria, CA, USA), and immunostained with Vectastain ABC

(Vector Laboratories, Inc., Burlingame, CA, USA). Antibodies against CD68 (1:100 dilution, 125212; Abcam), CD163 (1:100 dilution, 87099; Abcam), and NOS 2 (1:350 dilution, N-20; Santa Cruz Biotechnology) were incubated in TBS/Tween buffer overnight at 4 °C. Color was developed with 3,3'-diaminobenzidine tetrahydrochloride (Vector Laboratories, Inc.) and counterstained with H&E. An isotype immunoglobulin G (IgG) was used as negative control. CD68⁺ and CD163⁺ macrophage densities were assessed in five fields of view in the alveolar space by the point-counting technique, using a 100-point grid of known area (10⁴ μm²) attached to the eyepiece of the microscope [33]. The point-counting technique was assessed independently by one coauthor (VM), who was blinded to group allocation.

Enzyme-linked immunosorbent assay

Plasma levels of VEGF and platelet-derived growth factor (PDGF) (PeproTech, Rocky Hill, NJ, USA) were quantified 14 days after MSC therapy or saline administration in the CTRL-SAL, CTRL-MSC, MCT-SAL, and MCT-MSC groups. The results were normalized by total protein content by Bradford's technique, and expressed as picograms per microgram. All measurements were performed in accordance with manufacturer guidelines.

Expressions of interleukin-6, interleukin-10, pro-caspase-3, Bcl-2, survivin, Smad-1, GSK3B, VE-cadherin, vimentin, and α-actin

Quantitative real-time reverse transcription polymerase chain reaction (RT-PCR) was performed to assess biological markers of inflammation (interleukin (IL)-6 and IL-10) and apoptosis (procaspase-3, Bcl-2, and survivin) in lung tissue, and levels of small mothers against decapentaplegic homolog 1 (Smad-1), glycogen synthase kinase-3 beta (GSK3β), and markers of endothelial-mesenchymal transition (VE-cadherin, vimentin, and α-actin) in pulmonary artery tissue. Central slices of the lungs and proximal sections of the pulmonary artery were cut, collected in cryotubes, flash-frozen in liquid nitrogen, and stored at -80 °C. Total RNA was extracted (RNeasy Plus Mini Kit; Qiagen, Hilden, Germany) and the RNA concentration measured by spectrophotometry (Nanodrop ND-1000 system; Thermo Scientific, Wilmington, DE, USA). First-strand cDNA was synthesized from total RNA (Quantitec Reverse Transcription Kit; Qiagen). Relative mRNA levels were measured with a SYBR green detection system in an ABI 7500 real-time PCR analyzer (Applied Biosystems, Foster City, CA, USA). Samples were run in triplicate. For each sample, the expression of each gene was normalized to the acidic ribosomal phosphoprotein P0 (*36B4*) housekeeping gene [34] and expressed as fold change relative to CTRL-SAL, using the 2^{-ΔΔCt} method [35, 36]:

$$\Delta\text{Ct} = \text{Ct (reference gene)} - \text{Ct (target gene)}.$$

The following primers were used for lung tissue analyses: IL-6, 5'-CTC CGC AAG AGA CTT CCA G-3' (forward) and 5'-CTC CTC TCC GGA CTT GTG A-3' (reverse); IL-10, 5'-AGA AGG ACC AGC TGG ACA AC-3' (forward) and 5'-GTC GCA GCT GTA TCC AGA GG-3' (reverse); procaspase-3, 5'-GGC CGA CTT CCT GTA TGC-3' (forward) and 5'-GCG CAA AGT GAC TGG ATG-3' (reverse); Bcl-2, 5'-ATC GCT CTG TGG ATG ACT GA-3' (forward) and 5'-TGA TTT GAC CAT TTG CCT GA-3' (reverse); and survivin, 5'-AGC AGG TGG AAG AAC TGA CC-3' (forward) and 5'-AAA GCA AAA CCC CAA ATC ATC-3' (reverse). The following primers were used for pulmonary artery analyses: Smad-1, 5'-AGA ACC GAT TCT GCC TTG GG-3' (forward) and 5'-ACT CCG CAT ACA CCT CTC CT-3' (reverse); GSK3β, 5'-TCG CCA CTC GAG TAG AAG AAA' (forward) and 5'-ACT TTG TGA CTC AGG AGA ACT-3' (reverse); VE-cadherin, 5'-CAA TAC CGC CAA CAT CAC AG-3' (forward) and 5'-TGG TGA GGA TGC ACA GAA AG-3' (reverse); vimentin, 5'-CTG CCA AGA ACC TCC AGG AG-3' (forward) and 5'-ACT TCG CAG GTG AGT GAC TG-3' (reverse); and α-actin, 5'-GGA GAT GGC GTG ACT CAC AA-3' (forward) and 5'-TTG CGT TCT GGA GGA GCA AT-3' (reverse).

Expression of TGF-β and type I and III procollagen in lung fibroblasts

Lung fibroblasts were extracted and RT-PCR was performed to measure biological markers associated with fibrosis (transforming growth factor (TGF)-β, type I procollagen (PC-1), and type III procollagen (PC-3)). Lung fibroblasts were isolated as described previously [37]. Briefly, the right upper lung was removed, cut into small fragments, digested enzymatically in Liberase solution at 37 °C for 30 minutes, rinsed three times with warm DMEM/F12 media with 10% FBS, 1× penicillin/streptomycin, centrifuged at 524 × g, resuspended in complete DMEM/F12 media, transferred to a tissue culture dish, and, finally, placed in a humidified tissue culture incubator at 37 °C and 5% CO₂. After the cells reached 80–90% confluence, they were lysed and total RNA was extracted from frozen tissues using the RNeasy Plus Mini Kit (Qiagen), following the manufacturer's recommendations. Again, the RNA concentration was measured by spectrophotometry in Nanodrop ND-1000 (Thermo Scientific, Wilmington, DE, USA). First-strand cDNA was synthesized from total RNA using a Quantitec reverse transcription kit (Qiagen). Relative mRNA levels were measured with a SYBR green detection system using ABI 7500 real-time PCR (Applied Biosystems, Foster City, CA, USA). Samples were measured in triplicate. For each sample, the expression of each gene was normalized to *36B4* housekeeping gene expression [34] and expressed as

fold changes relative to CTRL-SAL, using the $2^{-\Delta\Delta Ct}$ method described earlier.

The following primers were used: TGF- β , 5'-ATA CGC CTG AGT GGC TGT C-3' (forward) and 5'-GCC CTG TAT TCC GTC TCC T-3' (reverse); PC-1 (α I), 5'-AGA AGT CTC AAG ATG GTG GCC G-3' (forward) and 5'-GGT CAC GAA CCA CGT TAG CAT C-3' (reverse); PC-3 (α I), 5'-CAG CTA TGG CCC TCC TGA TCT T-3' (forward) and 5'-GTA ATG TTC TGG GAG GCC CG-3' (reverse); and 36B4, 5'-CAA CCC AGC TCT GGA GAA AC-3' (forward) and 5'-CAA CCC AGC TCT GGA GAA AC-3' (reverse).

Statistical analysis

Each variable was tested for normality and variance using the Kolmogorov–Smirnov and Levene tests respectively. Data are presented as mean \pm SD unless otherwise specified. On day 14, parametric data were compared by a one-sample Student's *t* test ($\alpha < 0.05$). For comparisons between MCT at 14 days vs MCT-SAL and MCT-MSc at 28 days, paired *t* tests were used ($\alpha < 0.05$). On day 28, parametric and nonparametric data were analyzed by multiple Student *t* tests and Wilcoxon signed-rank tests respectively, followed by Bonferroni's correction (adjusted $\alpha^* < 0.0167$ for three comparisons: CTRL-SAL vs CTRL-MSc, CTRL-SAL vs MCT-SAL, and MCT-SAL

vs MCT-MSc). The Bonferroni-adjusted significance level was used to counteract multiple comparisons [38]. Pearson's correlations were calculated and $p < 0.05$ was adopted as significant. All tests were performed in GraphPad Prism version 6.01 (Graph-Pad Software, La Jolla, CA, USA).

Results

Echocardiography and hemodynamic measurements

Fourteen days after MCT induction of PAH, the PAT/PET ratio was reduced in PAH animals compared to CTRL, suggesting pulmonary hypertension (0.38 ± 0.09 vs 0.47 ± 0.08 respectively; $p = 0.016$). The ratio remained lower at day 28 (MCT-SAL, 0.27 ± 0.07 vs CTRL-SAL, 0.40 ± 0.05 ; $p < 0.001$). In the MCT-SAL group, the PAT/PET ratio was lower at day 28 compared to day 14 ($p = 0.03$). On the other hand, in the MCT-MSc group the PAT/PET ratio did not differ between days 14 and 28 ($p = 0.54$), which may suggest mitigation of the course of PAH (Fig. 1a).

On day 28, MCT-SAL animals exhibited higher RVSP (39 ± 2 mmHg vs 24 ± 1 mmHg respectively; $p < 0.0001$) (Fig. 1b) and RV dp/dtmax (1422 ± 144 mmHg/s vs 755 ± 166 mmHg/s respectively; $p < 0.0001$) (Fig. 1c) than CTRL-SAL animals. After MSc therapy, RVSP and RV dp/dtmax reduced in the MCT-MSc group compared to

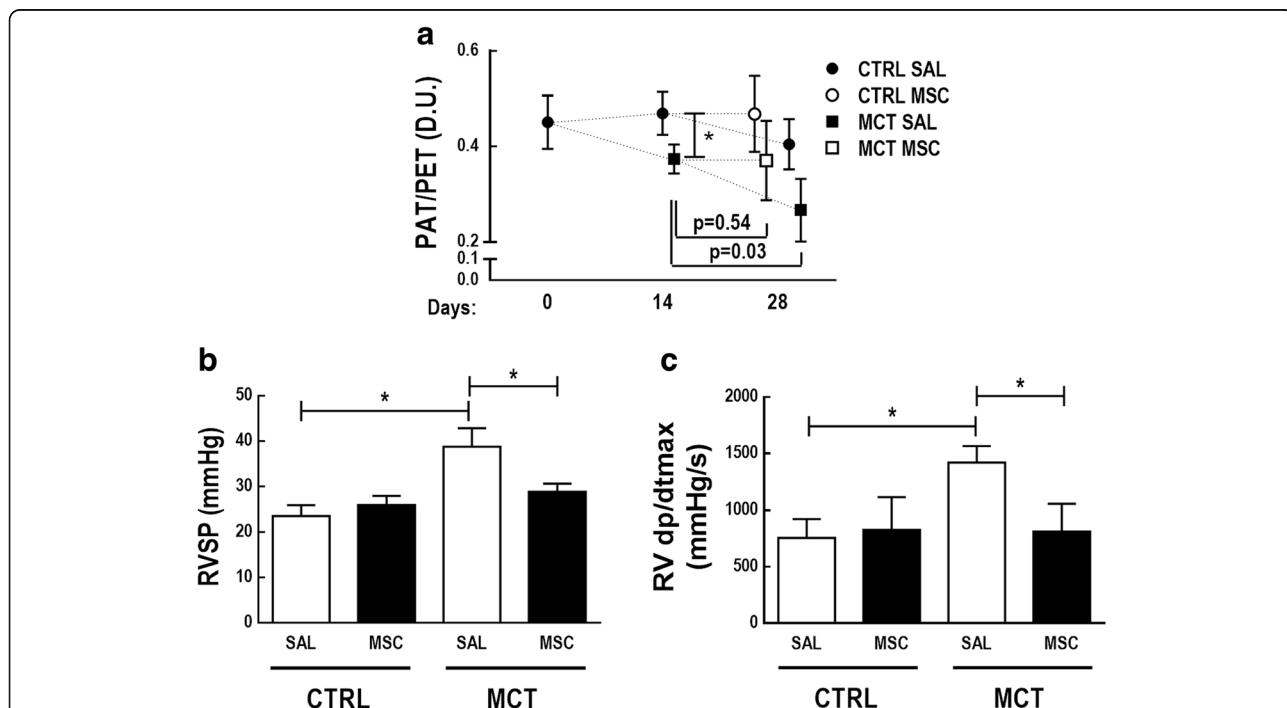


Fig. 1 Progression of echocardiographic parameters. Echocardiography performed at 0, 14, and 28 days after injection of SAL (closed circle) or MCT (closed square). Open circle and square symbols represent CTRL and MCT animals respectively. (a) PAT/PET ratio. * $p < 0.05$. (b) Right ventricular systolic pressure (RVSP) at day 28. (c) Right ventricular contraction rate (RV dp/dtmax) at day 28. Values represent mean \pm SD of seven animals/group. Comparisons by Student's *t* test followed by Bonferroni's procedure for three comparisons (* $p < 0.0167$). CTRL control, MCT monocrotaline, SAL saline, D.U. dimensionless units, PAT pulmonary acceleration time, PET pulmonary ejection time

MCT-SAL (RVSP: MCT-MSC vs MCT-SAL, 29 ± 1 mmHg vs 39 ± 2 mmHg respectively, $p < 0.001$; RV dp/dtmax: MCT-MSC vs MCT-SAL, 812 ± 244 mmHg/s vs 1422 ± 144 mmHg/s respectively, $p = 0.0006$) (Fig. 1b, c).

Endothelial dysfunction of pulmonary hypertension

Arteries from MCT-SAL animals exhibited less of a vasodilator response to increasing doses of ACh compared to those of CTRL-SAL animals ($48 \pm 5\%$ vs $64 \pm 2\%$ respectively). This result was reinforced by calculation of the effective dose 50 (ED50) for ACh-induced dilation in both groups, in which CTRL-SAL animals showed a lower ED50 (-6.99) than MCT-SAL animals (-6.11). After MSC therapy, no additional vasodilator response of the pulmonary arterial rings was observed in MCT animals (Additional file 1: Figure S1).

Evaluation of pulmonary arteriopathy

On OM analysis, the following features were altered in MCT-SAL compared to CTRL-SAL animals: medial hypertrophy (pre-acinar, $p = 0.006$; intra-acinar, $p = 0.01$), concentric laminar intimal thickening (pre-acinar, $p = 0.006$; intra-acinar, $p = 0.006$), plexiform-like lesions (pre-acinar, $p = 0.012$; intra-acinar, $p = 0.006$), and dilatation lesions (pre-acinar, $p = 0.006$; intra-acinar, $p = 0.006$) (Table 1, Fig. 2). MSC therapy attenuated some histologic features, such as plexiform-like lesions in the pre-acinar artery ($p = 0.008$), concentric laminar intimal thickening in the intra-acinar artery ($p = 0.008$), and medial hypertrophy for both arteries (pre-acinar, $p = 0.008$; intra-acinar, $p = 0.008$) (Fig. 2).

On TEM analysis, MCT-SAL animals showed concentric laminar intimal thickening and prominent basement membrane in the pre-acinar and intra-acinar pulmonary arteries. In addition, MCT-SAL animals exhibited external fibronectin fibers and intracellular actin microfilaments. After MSC therapy, concentric laminar intimal and basement-membrane thickening decreased (Additional file 1: Figure S2).

MCT-SAL animals had higher CD68⁺ and CD163⁺ cell counts than CTRL-SAL (16 (14–17) vs 2 (1, 2),

$p < 0.0001$; and 3 (3–4.75) vs 2 (1, 2), $p < 0.0001$ respectively). MCT-MSC animals, compared to MCT-SAL, exhibited reductions in CD68⁺ cell counts (4 (3–4.5) vs 16 (14–17), $p = 0.016$), as well as increased CD163⁺ cell counts (11 (10–12.5) vs 3 (3–4.75), $p = 0.008$) (Fig. 3).

VEGF content was higher in MCT-SAL animals than CTRL-SAL (12 (9.75–15) vs 2 (1.25–2) respectively; $p = 0.002$) (Fig. 4). Compared to SAL, MSC therapy was able to reduce the arteriolar VEGF content ($p < 0.0001$). MCT-SAL animals had higher smooth muscle cell hypertrophy and hyperplasia scores than CTRL-SAL animals (12 (12–15) vs 0 (0–0) respectively; $p = 0.002$). MSC therapy attenuated smooth muscle cell hypertrophy and hyperplasia, as demonstrated by significantly lower scores in MCT-MSC compared to MCT-SAL animals ($p = 0.003$) (Fig. 4).

Quantification of lung collagen and mRNA expression of inflammatory, apoptotic, and profibrotic mediators and markers of cell proliferation and endothelial–mesenchymal transition

MCT-SAL animals showed higher levels of collagen in lung tissue compared to CTRL-SAL animals (36 ± 2 μ g vs 25 ± 3 μ g respectively; $p = 0.0145$), and MSC therapy reduced collagen content in MCT animals (27 ± 3 μ g vs 36 ± 2 μ g respectively; $p = 0.0169$) (Fig. 5a).

MCT-SAL animals showed higher IL-6 ($p < 0.0167$) and survivin mRNA expression in lung tissue compared to CTRL-SAL. In addition, Smad-1 and GSK3 β mRNA expressions were higher in MCT-SAL than CTRL-SAL animals ($p < 0.0167$ for both). In pulmonary artery tissue, VE-cadherin mRNA expression was lower, while vimentin and α -actin were higher in MCT-SAL animals compared to CTRL-SAL.

MSC therapy decreased IL-6, Bcl-2, and survivin mRNA expression ($p < 0.0167$ for all) and increased procaspase-3 mRNA expression in lung tissue ($p < 0.0167$) (Fig. 6a–e). In pulmonary artery tissue, levels of GSK3 β , but not Smad-1, mRNA were lower in MCT-MSC than in MCT-SAL animals (Fig. 7a, b). MCT-MSC animals showed increased VE-cadherin mRNA expression but reduced

Table 1 Histopathological score for pulmonary arterial hypertension

	Pre-acinar artery			Intra-acinar artery		
	Medial hypertrophy	Concentric laminar intimal thickening	Dilatation lesions	Medial hypertrophy	Concentric laminar intimal thickening	Dilatation lesions
CTRL-SAL	1 (1–1)	1 (1–1)	0 (0–0)	0 (0–0)	0 (0–0)	0 (0–0)
CTRL-MSC	1 (1–1)	1 (1–1)	0 (0–0)	0 (0–0)	0 (0–0)	0 (0–0)
MCT-SAL	4 (4–4)*	4 (4–4)*	2 (1–3)*	3 (2–4)*	3 (2–4)*	2 (2–2)*
MCT-MSC	2 (1–3) [†]	2 (2–2)	1 (0–1)	2 (1–3) [†]	2 (0–2) [†]	2 (1–3)

Classification of vasculopathies in pulmonary hypertension. Values presented as median (interquartile range) of seven animals/group

CTRL control, MCT monocrotaline, SAL saline

*Significantly different from CTRL-SAL group ($p < 0.0167$)

[†]Significantly different from MCT-SAL group ($p < 0.0167$)

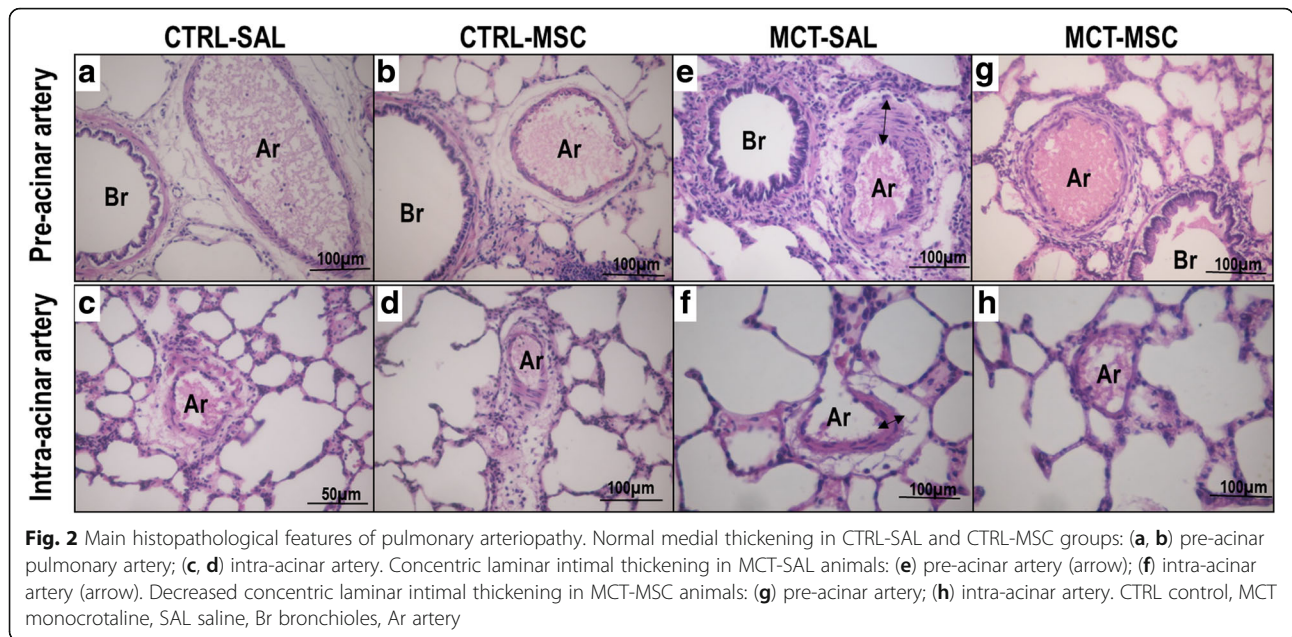


Fig. 2 Main histopathological features of pulmonary arteriopathy. Normal medial thickening in CTRL-SAL and CTRL-MSC groups: (a, b) pre-acinar pulmonary artery; (c, d) intra-acinar artery. Concentric laminar intimal thickening in MCT-SAL animals: (e) pre-acinar artery (arrow); (f) intra-acinar artery (arrow). Decreased concentric laminar intimal thickening in MCT-MSC animals: (g) pre-acinar artery; (h) intra-acinar artery. CTRL control, MCT monocrotaline, SAL saline, Br bronchioles, Ar artery

mRNA expression of mesenchymal markers such as vimentin and α -actin compared to MCT-SAL animals (Fig. 7c–e).

In lung fibroblasts, MCT-SAL compared to CTRL-SAL animals showed higher procollagen I, procollagen III, and TGF- β mRNA expressions, which were reduced in the MCT-MSC group in comparison to MCT-SAL ($p < 0.0001$) (Fig. 5b–d).

Enzyme-linked immunosorbent assay for plasma VEGF and PDGF

On day 28, MCT-SAL animals had lower plasma VEGF levels compared to CTRL-SAL (29.5 ± 23.0 pg/ μ g vs 117.2 ± 39.4 pg/ μ g, $p < 0.0167$). In MCT-MSC animals,

plasma VEGF was lower than in MCT-SAL (1.9 ± 1.3 pg/ μ g vs 29.5 ± 23.0 pg/ μ g, $p < 0.0167$). PDGF levels did not differ among groups (Table 2).

Discussion

In the monocrotaline-induced experimental model of PAH used herein, MSC therapy reduced right ventricular systolic pressure, histological damage and smooth muscle cell thickening, CD68⁺ macrophage density in lung tissue, lung arteriolar and plasma VEGF levels, total lung collagen, mRNA levels of procollagen type I, type III, and TGF- β in lung fibroblast culture, and inflammatory and anti-apoptotic markers in lung tissue. MSC therapy increased proapoptotic mediators in lung tissue

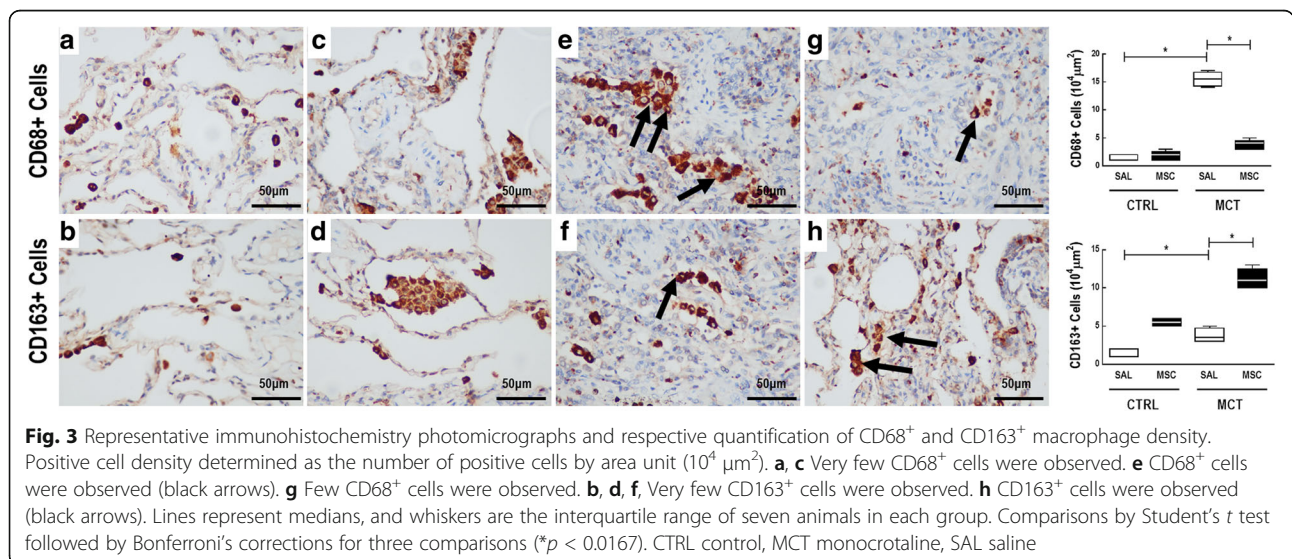
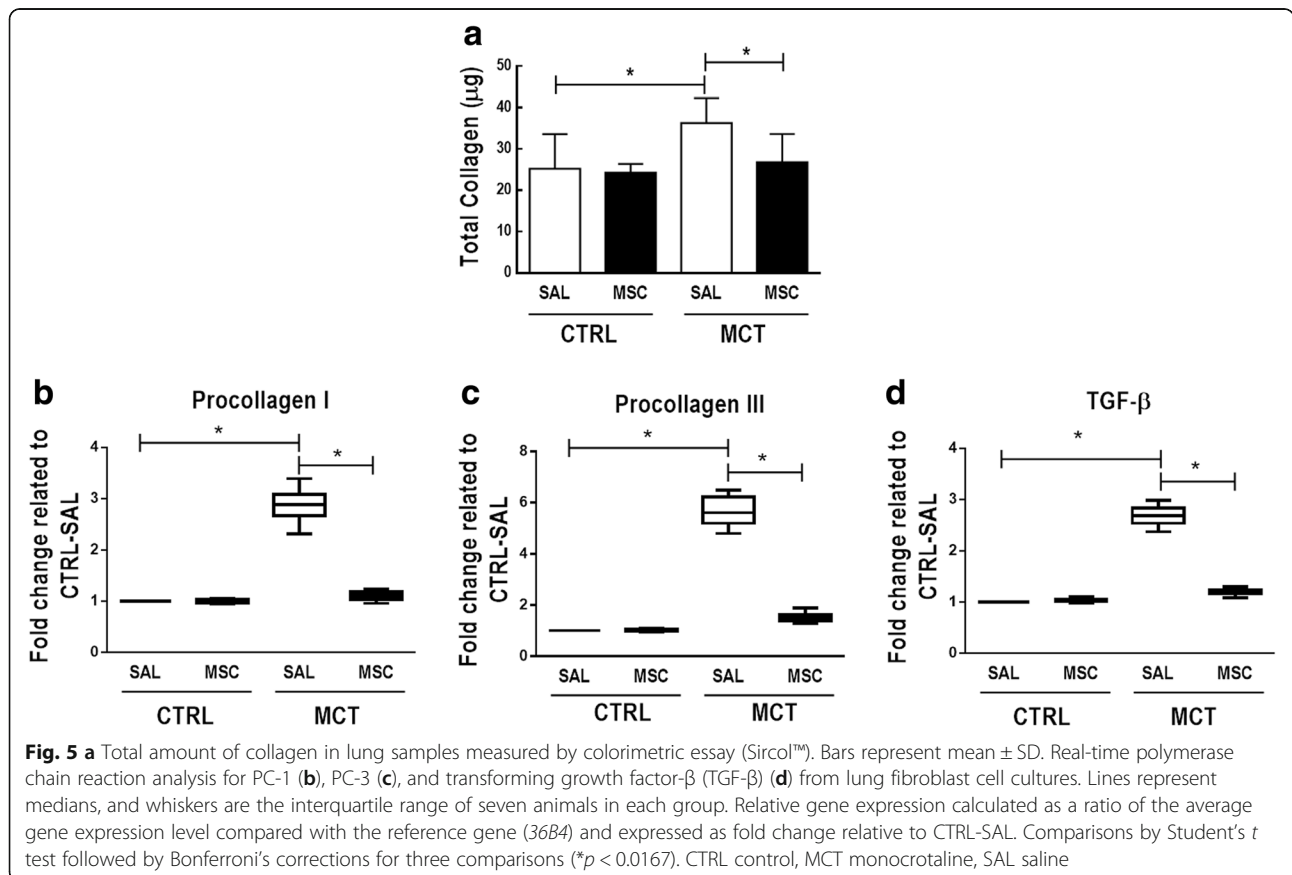
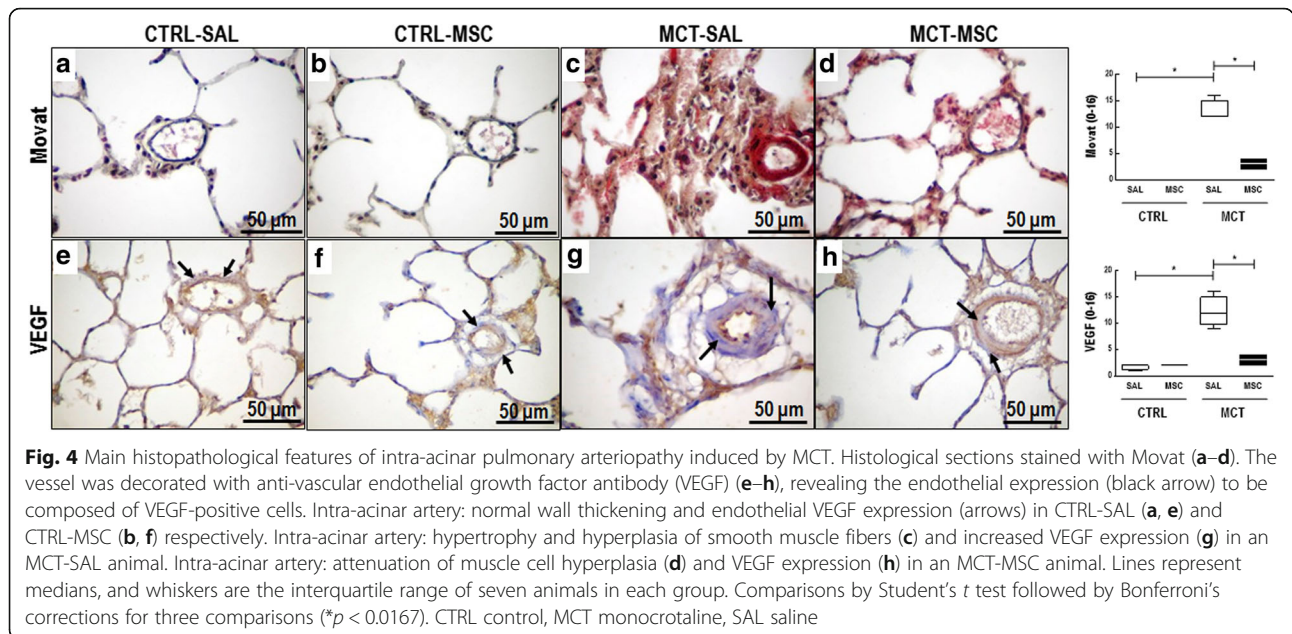
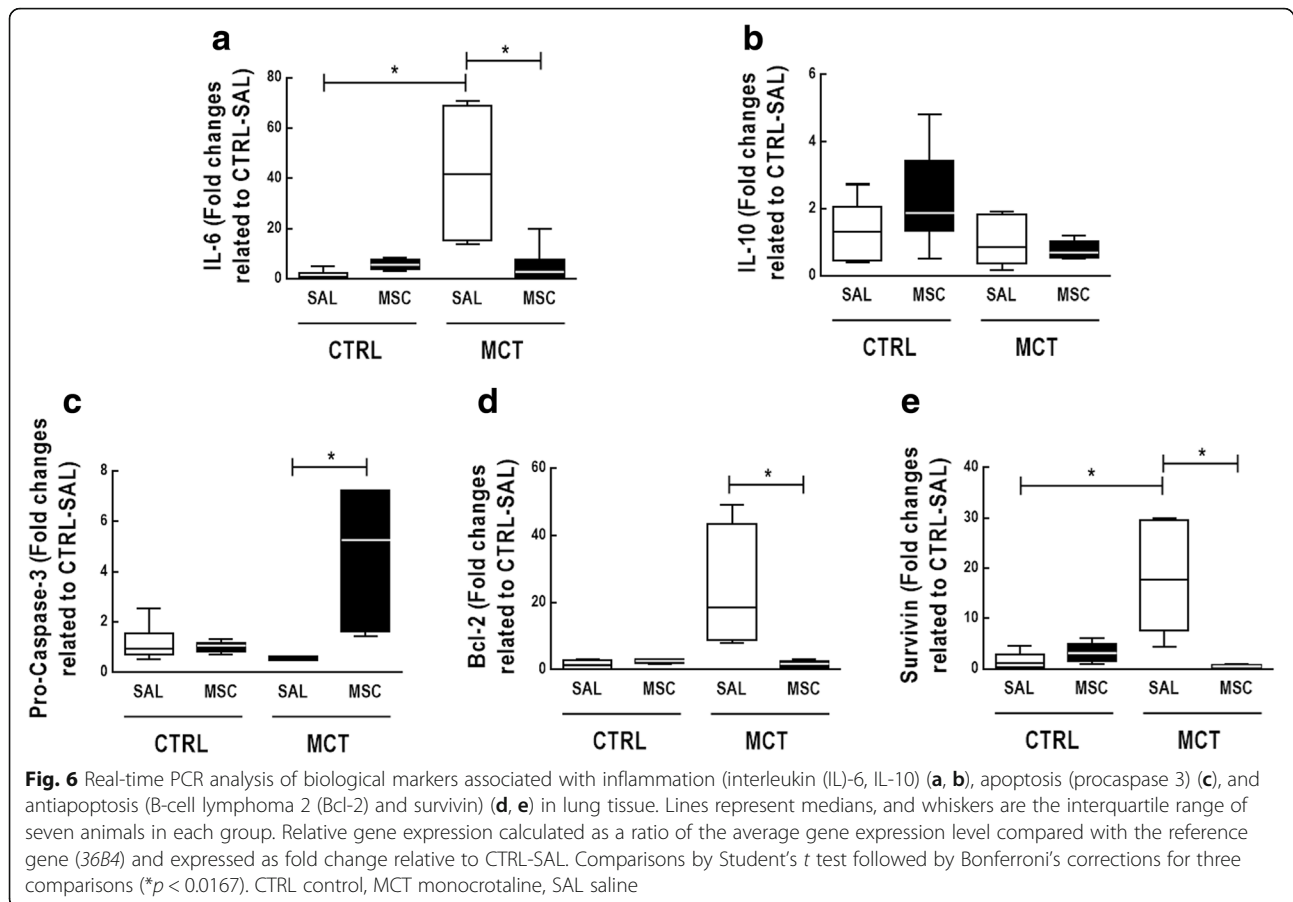


Fig. 3 Representative immunohistochemistry photomicrographs and respective quantification of CD68⁺ and CD163⁺ macrophage density. Positive cell density determined as the number of positive cells by area unit ($10^4 \mu\text{m}^2$). a, c Very few CD68⁺ cells were observed. e CD68⁺ cells were observed (black arrows). g Few CD68⁺ cells were observed. b, d, f, Very few CD163⁺ cells were observed. h CD163⁺ cells were observed (black arrows). Lines represent medians, and whiskers are the interquartile range of seven animals in each group. Comparisons by Student's *t* test followed by Bonferroni's corrections for three comparisons ($*p < 0.0167$). CTRL control, MCT monocrotaline, SAL saline





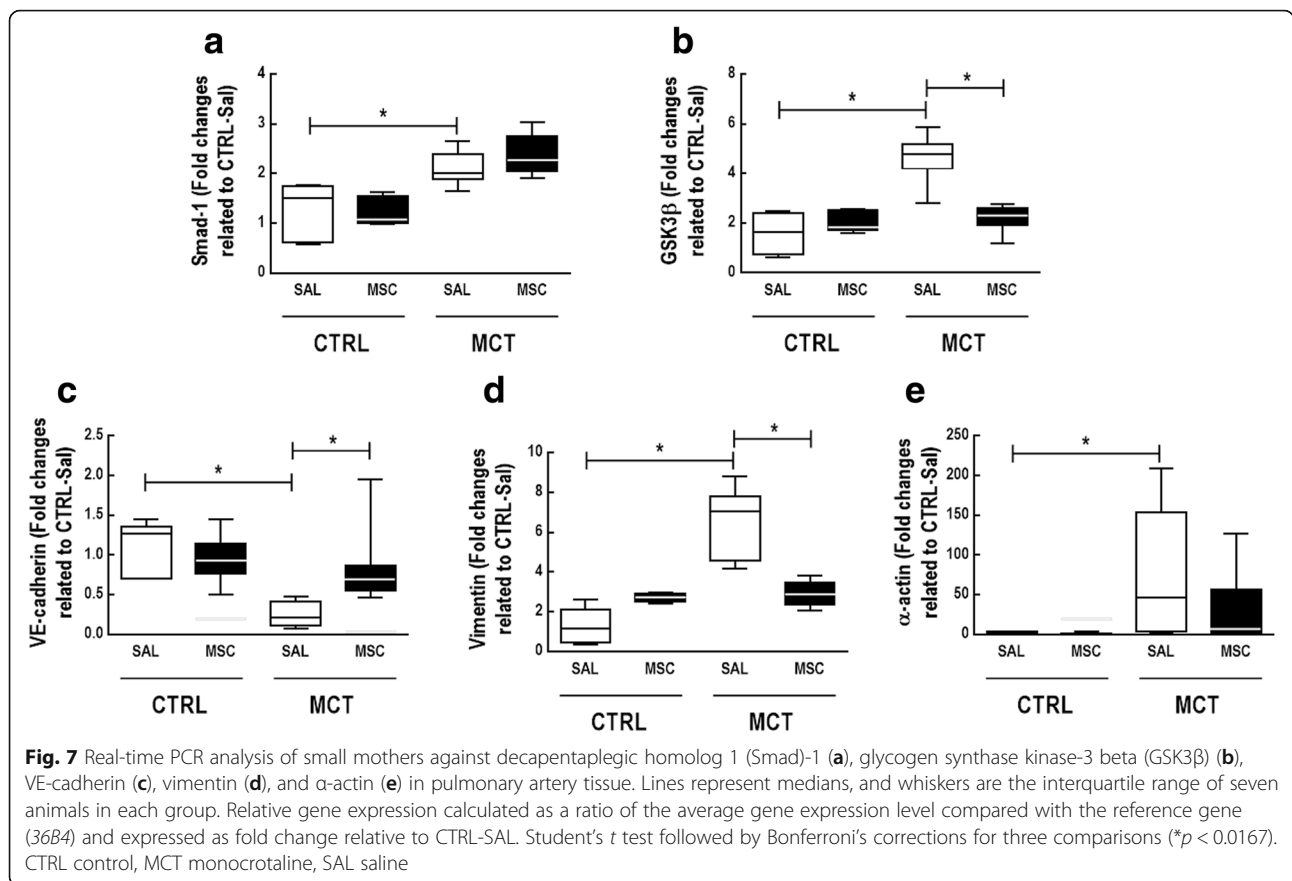
while decreasing cell proliferation markers in pulmonary artery tissue, suggesting minimization of the heightened proliferative state observed in monocrotaline-induced PAH. Furthermore, MSC therapy may act through the endothelial–mesenchymal transition, as measured by gene expression in the pulmonary artery.

Monocrotaline has been widely used to induce PAH in small rodents [6, 39, 40]. In this line, we observed several pathophysiological features associated with PAH in animals exposed to MCT, such as an increase in RV hypertrophy index (RV/LV + S; data not shown), RVSP, and medial hypertrophy and concentric laminar intimal thickening in both pre-acinar and intra-acinar arteries. Since we were concerned about the functional and histopathological features of PAH, the usage of MCT would fit with our research question, as well as with the respective time course alterations [41] after MSC treatment.

Cell therapy and inflammation

In the present study, we used 10^5 adipose-derived MSCs (a lower dosage than in previous studies [16]), obtained from healthy animals, and observed an attenuation of inflammatory markers, including IL-6, as in previous pre-clinical studies using MSCs in PAH animals. IL-6 is a key

factor that facilitates a shift in pericytes from the quiescent state into their contractile, hyperproliferative state [42], which would increase pulmonary vascular resistance in PAH. Nevertheless, the association of IL-6 with macrophage polarization in PAH has not been clear. By modulating macrophage polarization and therefore IL-6 production, induced pluripotent stem cell (iPSC)-based therapy has been shown to reduce inflammation and M1 phenotype subpopulations in human polarized macrophages in vitro [11]. Herein, we observed not only IL-6 and CD68⁺ macrophage attenuation but also an increase in the CD163⁺ macrophage subpopulation in vivo. Although we did not evaluate the precise mechanism of mitigation of inflammatory process, it may rely on inhibition of the NF- κ B pathway [11]. By modulating the M1 phenotype and IL-6 mRNA expression, MSCs may minimize the intense proliferation observed in PAH. In this line, we observed a reduction in mRNA expression of Bcl-2 and survivin, which are known to have antiapoptotic properties [43], leading to cell survival, and intense remodeling [44]. Likewise, we observed a relative increase in procaspase-3 mRNA expression after MSC therapy in MCT animals, which, by increasing apoptosis, may counteract the intense cell proliferation observed in PAH.



Cell therapy and remodeling

Previous studies have reported a reduction in vascular remodeling after MSC therapy [16–18, 20]. Despite using a lower dose of MSCs than prior studies [16–20], we observed a reduction in the remodeling process. Furthermore, previous studies have focused only on pulmonary vessel wall thickness, which is a more general measurement [16–18, 20]. Conversely, we were interested in the main histopathological features of PAH seen in the pre-acinar and intra-acinar pulmonary arteries [21]. In the pre-acinar arteries, after MSC therapy, we observed a reduction in medial hypertrophy and plexiform-like lesions, which represent specific features

in PAH [21, 45], while in the intra-acinar arteries there was a reduction in medial hypertrophy and concentric laminar intimal thickening. Similar results were observed after MSC therapy in atherosclerosis lesions [46]. In pulmonary artery smooth muscle cells, GSK3β represents a mediator of the Akt pathway toward cell proliferation [47]. It has been shown that GSK3β increases in monocrotaline-induced PAH, and its levels are negatively modulated by HIV protease inhibitors in line with decreased proliferation in pulmonary arteries [48]. We observed a reduction in GSK3β but not Smad-1 levels in pulmonary artery tissue after MSC therapy. This suggests that MSCs may interfere with the Akt–GSK3β axis, one of the major non-SMAD signaling pathways [49] toward cell proliferation [47]. Since Smad-1 belongs to the bone marrow protein receptor (BMPR)/Smad signaling pathway, the lack of effect observed after MSC therapy may be explained by the minor role of BMPR-2 in pulmonary artery smooth muscle cells in monocrotaline-induced PAH [50]. We also isolated fibroblast cells after MSC therapy in order to provide further support to cell therapy and remodeling. Fibroblast cells can change their phenotype into myofibroblasts, acting on mRNA expression of procollagen and TGF-β, which have been associated with intimal arterial injury during PAH [2]

Table 2 Plasma levels of biomarkers

	CTRL		MCT	
	SAL	MSC	SAL	MSC
VEGF (pg/μg)	117.2 ± 39.4	135.9 ± 156.3	29.5 ± 23.0 [#]	1.9 ± 1.3 [†]
PDGF (pg/μg)	508.7 ± 205.2	520.7 ± 338.0	343.0 ± 239.0	458.1 ± 365.9

Plasma levels of vascular endothelial growth factor (VEGF) and platelet-derived growth factor (PDGF) at 28 days. Results normalized by total protein content (Bradford's technique) as picograms per microgram. Values presented as mean ± SD of seven animals/group

CTRL control, MCT monocrotaline, SAL saline

[#]Significantly different from CTRL-SAL at 28 days ($p < 0.0167$)

[†]Significantly different from MCT-SAL at 28 days ($p < 0.0167$)

and intense endothelial-to-mesenchymal transition after MCT administration [51]. We observed a reduction in TGF- β , procollagen type I, and procollagen type III mRNA expression in lung fibroblast cell cultures after MSC therapy. Previous studies have demonstrated that MSC-conditioned medium significantly downregulates procollagen type I and procollagen type III mRNA expression, which reflects the paracrine antifibrotic effects of MSCs [52]. In addition, along with increased VE-cadherin, we also detected reductions in vimentin and α -actin, which suggests that the change from an endothelial into a mesenchymal phenotype observed in PAH [51] was dampened after MSC administration.

Cell therapy and growth factors

Because of the controversial roles of different growth factors in PAH [53], we decided to evaluate VEGF and PDGF levels over time in plasma and small pulmonary vessels. VEGF is the most important factor regulating both physiological and pathogenic angiogenesis [54]. Serum and endothelial levels of VEGF, as well as VEGF receptor 2 (VEGFR-2) expression, are known to be increased in PAH patients [4, 55]. In PAH pathogenesis, VEGF may act as a potent stimulator of the disordered angiogenic process through a phenotype shift of pulmonary vascular smooth muscle cells from a quiescent state into a proliferative and antiapoptotic profile [7]. In this line, balancing this pathway might provide a desirable therapeutic avenue. In ischemia–reperfusion injury [56], MSC therapy has been shown to increase lung tissue VEGF levels, which was followed by vascularization and angiogenesis in vitro [56, 57]. In contrast, after MSC therapy, we observed lower VEGF levels in both plasma and small pulmonary vessels. The relationship between inflammation and angiogenesis may explain these contradictory findings. MSCs reduced inflammation by changing the macrophage phenotype from M1 (proinflammatory) toward M2 (anti-inflammatory) and, consequently, reducing IL-6 mRNA expression. In this scenario, lower proliferation and angiogenesis and, therefore, lower VEGF levels are to be expected. In addition, at the time of MSC administration (i.e., on day 14), circulating levels of VEGF were higher in MCT compared to CTRL animals. Administration of MSCs on day 14 would balance out the intense proliferative state and might act at the endothelial niche by the interaction of pericytes and the innate immune system [58], by increasing plasticity [59], and by balancing pulmonary vessel density [60].

In contrast, since no major alterations in plasma PDGF levels were observed, we did not evaluate PDGF in lung tissue after MSC therapy. Therefore, the observed reduction in proliferative status may be largely attributable to VEGF downregulation. It should be pointed out that the effects of MSCs may be attributable to their paracrine

effects rather than to their presence in the injured lung area, since beneficial effects have been observed after administration of MSC-conditioned medium [61] and extracellular vesicles [62, 63] in PAH and other respiratory diseases.

Cell therapy and functional parameters

In this experiment, MSC therapy may have improved hemodynamics, as represented by a reduction in RVSP, mainly due to attenuation of vascular remodeling [64]. Accordingly, we did not observe a significant vasodilatory response of the pulmonary arterial rings after MSC therapy, which provides further evidence of this effect. Previous studies have reported reductions in pulmonary arterial pressures after MSC administration, followed by a vasodilatory response to ACh [19]. The methods used in these prior investigations were based on the in-vivo setting, and involved i.v. injection of acetylcholine after administration of a prostaglandin agonist [19]. This has several limitations, including the fact that the systemic effects of ACh and prostaglandin might prevent proper measurement of endothelial dysfunction and that ACh dosages used in vivo are fourfold higher than those used in the present study during in-vitro measurements. In addition, the in-vitro method employed in our study has been widely used in prior research [65, 66].

Limitations

The limitations of the present study must be taken into account. First, instead of performing repeated punctures for direct (invasive) measurement of RV pressures, we used echocardiography to choose the best timing for therapeutic interventions, according to indirect but reliable markers of pulmonary hypertension, such as the PAT/PET ratio [27, 67, 68]. Second, monocrotaline-induced PAH is not able to mimic the entire complex features observed in human PAH. Nevertheless, it is a well-established model of moderately severe PAH [69] and has been widely used both to elucidate its pathophysiological mechanisms [70, 71] and to propose new therapeutic interventions [65]. Third, we chose to analyze the roles of VEGF and PDGF specifically because these mediators are associated with angiogenesis [8, 72], as shown in prior studies with the MCT experimental model [71] and in human patients with PAH [2]. Nevertheless, we cannot rule out a role for other growth factors.

Conclusion

In experimental monocrotaline-induced PAH, MSC therapy improved hemodynamics by mitigating lung vascular remodeling. These beneficial effects seem to be associated with an increase in proapoptotic markers, modulation of endothelial–mesenchymal transition, and decrease in cell proliferation markers and inflammation due to reduction in the M1 macrophage subpopulation.

Additional file

Additional file 1: Determination of pulmonary artery function and Transmission electron microscopy of pulmonary arteries. (DOCX 3690 kb)

Abbreviations

Ach: Acetylcholine; CTRL: Control; GSK3 β : Glycogen synthase kinase-3beta; H&E: Hematoxylin–eosin; i.p.: Intraperitoneally; IL: Interleukin; iPSC: Induced pluripotent stem cell; MCT: Monocrotaline; MSC: Mesenchymal stromal cell; OM: Optical microscopy; PAH: Pulmonary arterial hypertension; PAT: Pulmonary artery acceleration time; PC-1: Type I procollagen; PC-3: Type III procollagen; PDGF: Platelet-derived growth factor; PET: Pulmonary artery ejection time; Phe: Phenylephrine; RT-PCR: Real-time reverse transcription polymerase chain reaction; RV dp/dtmax: RV contraction rate; RV/LV + S: RV hypertrophy index; RVSP: Right ventricular systolic pressure; SAL: Saline; Smad-1: Small mothers against decapentaplegic homolog 1; TEM: Transmission electron microscopy; TGF: Transforming growth factor; VEGF: Vascular endothelial growth factor

Acknowledgements

The authors would like to acknowledge Mr Andre Benedito da Silva for animal care, Mrs Ana Lucia Neves da Silva for her help with microscopy, and Mrs Moira Elizabeth Schöttler and Mr Filipe Vasconcellos for their assistance in editing the manuscript.

Funding

This study was supported by the Brazilian Council for Scientific and Technological Development (CNPq), the Rio de Janeiro State Research Foundation (FAPERJ), the Department of Science and Technology (DECIT)/Brazilian Ministry of Health (MS), the Coordination for the Improvement of Higher Education Personnel (CAPES), and the National Institute of Science and Technology for Regenerative Medicine (INCT-REGENERA).

Availability of data and materials

The datasets generated and/or analyzed during the current study are available from the corresponding author on reasonable request.

Authors' contributions

LDM, NSF, NGB, JSDS, SCA, FFC, NR, GZ-S, PRMR, and PLS were involved in the design and conduction of the study, data collection, and manuscript writing. LDM, SCA, and FFC performed isolation and culture of MSCs. LDM, NSF, NGB, JSDS, and FFC performed the experiments. VM and VLC participated in electron microscopy analysis and manuscript writing. LDM, FFC, GZ-S, PRMR, and PLS were involved in the design of the study, data analysis, and manuscript writing. TPF and PMS participated in collagen analysis and manuscript writing. All authors read and approved the final version of the manuscript.

Ethics approval

This study was approved by the Animal Ethics Committee of the Health Sciences Center, Federal University of Rio de Janeiro (CEUA 114/14). All animals received humane care in compliance with the "Principles of Laboratory Animal Care" formulated by the National Society for Medical Research and the US National Research Council "Guide for the Care and Use of Laboratory Animals".

Competing interests

The authors declare that they have no competing interests.

Publisher's Note

Springer Nature remains neutral with regard to jurisdictional claims in published maps and institutional affiliations.

Author details

¹Laboratory of Pulmonary Investigation, Carlos Chagas Filho Biophysics Institute, Federal University of Rio de Janeiro, Centro de Ciências da Saúde, Avenida Carlos Chagas Filho, s/n, Bloco G-014, Ilha do Fundão, Rio de Janeiro, RJ 21941-902, Brazil. ²National Institute of Science and Technology for Regenerative Medicine, Rio de Janeiro, RJ, Brazil. ³Laboratory of Cardiovascular Pharmacology, Federal University of Rio de Janeiro, Rio de Janeiro, RJ, Brazil. ⁴Department of Physiology, Fluminense Federal University, Niterói, RJ, Brazil. ⁵Laboratory of Inflammation, Oswaldo Cruz Institute—Oswaldo Cruz Foundation, Rio de Janeiro, RJ, Brazil. ⁶Laboratory of

Histomorphometry and Lung Genomics, University of São Paulo Faculty of Medicine, São Paulo, SP, Brazil.

Received: 28 June 2017 Revised: 29 August 2017

Accepted: 12 September 2017 Published online: 03 October 2017

References

- Lai YC, Potoka KC, Champion HC, Mora AL, Gladwin MT. Pulmonary arterial hypertension: the clinical syndrome. *Circ Res*. 2014;115:115–30.
- Schermlay RT, Ghofrani HA, Wilkins MR, Grimminger F. Mechanisms of disease: pulmonary arterial hypertension. *Nat Rev Cardiol*. 2011;8:443–55.
- Voelkel NF, Bogaard HJ, Gomez-Arroyo J. The need to recognize the pulmonary circulation and the right ventricle as an integrated functional unit: facts and hypotheses (2013 Grover Conference series). *Pulm Circ*. 2015;5:81–9.
- Eddahibi S, Humbert M, Sediame S, Chouaid C, Partovian C, Maitre B, et al. Imbalance between platelet vascular endothelial growth factor and platelet-derived growth factor in pulmonary hypertension. Effect of prostacyclin therapy. *Am J Respir Crit Care Med*. 2000;162:1493–9.
- Tuder RM, Abman SH, Braun T, Capron F, Stevens T, Thistlethwaite PA, et al. Development and pathology of pulmonary hypertension. *J Am Coll Cardiol*. 2009;54:S3–9.
- Stenmark KR, Meyrick B, Galie N, Mooi WJ, McMurtry IF. Animal models of pulmonary arterial hypertension: the hope for etiological discovery and pharmacological cure. *Am J Physiol Lung Cell Mol Physiol*. 2009;297:L1013–32.
- Pullamsetti SS, Schermlay R, Ghofrani A, Weissmann N, Grimminger F, Seeger W. Novel and emerging therapies for pulmonary hypertension. *Am J Respir Crit Care Med*. 2014;189:394–400.
- Hassoun PM, Mouthon L, Barbera JA, Eddahibi S, Flores SC, Grimminger F, et al. Inflammation, growth factors, and pulmonary vascular remodeling. *J Am Coll Cardiol*. 2009;54:S10–9.
- Abe K, Toba M, Alzoubi A, Ito M, Fagan KA, Cool CD, et al. Formation of plexiform lesions in experimental severe pulmonary arterial hypertension. *Circulation*. 2010;121:2747–54.
- Voelkel NF, Gomez-Arroyo J. The role of vascular endothelial growth factor in pulmonary arterial hypertension. The angiogenesis paradox. *Am J Respir Cell Mol Biol*. 2014;51:474–84.
- Huang WC, Ke MW, Cheng CC, Chiou SH, Wann SR, Shu CW, et al. Therapeutic benefits of induced pluripotent stem cells in monocrotaline-induced pulmonary arterial hypertension. *PLoS One*. 2016;11:e0142476.
- Reinders ME, Sho M, Izawa A, Wang P, Mukhopadhyay D, Koss KE, et al. Proinflammatory functions of vascular endothelial growth factor in alloimmunity. *J Clin Invest*. 2003;112:1655–65.
- Galie N, Ghofrani HA, Torbicki A, Barst RJ, Rubin LJ, Badesch D, et al. Sildenafil citrate therapy for pulmonary arterial hypertension. *N Engl J Med*. 2005;353:2148–57.
- Patel N, Tahara SM, Malik P, Kalra VK. Involvement of miR-30c and miR-301a in immediate induction of plasminogen activator inhibitor-1 by placental growth factor in human pulmonary endothelial cells. *Biochem J*. 2011;434:473–82.
- Wang XX, Zhang FR, Shang YP, Zhu JH, Xie XD, Tao QM, et al. Transplantation of autologous endothelial progenitor cells may be beneficial in patients with idiopathic pulmonary arterial hypertension: a pilot randomized controlled trial. *J Am Coll Cardiol*. 2007;49:1566–71.
- Rathinasabapathy A, Bruce E, Espejo A, Horowitz A, Sudhan DR, Nair A, et al. Therapeutic potential of adipose stem cell-derived conditioned medium against pulmonary hypertension and lung fibrosis. *Br J Pharmacol*. 2016;173:2859–79.
- Eguchi M, Ikeda S, Kusumoto S, Sato D, Koide Y, Kawano H, et al. Adipose-derived regenerative cell therapy inhibits the progression of monocrotaline-induced pulmonary hypertension in rats. *Life Sci*. 2014;118:306–12.
- Angelini A, Castellani C, Ravara B, Franzin C, Pozzobon M, Tavano R, et al. Stem-cell therapy in an experimental model of pulmonary hypertension and right heart failure: role of paracrine and neurohormonal milieu in the remodeling process. *J Heart Lung Transplant*. 2011;30:1281–93.
- Baber SR, Deng W, Master RG, Bunnell BA, Taylor BK, Murthy SN, et al. Intratracheal mesenchymal stem cell administration attenuates monocrotaline-induced pulmonary hypertension and endothelial dysfunction. *Am J Physiol Heart Circ Physiol*. 2007;292:H1120–8.
- Umar S, de Visser YP, Steendijk P, Schutte CI, el Laghmani H, Wagenaar GT, et al. Allogenic stem cell therapy improves right ventricular function by improving lung pathology in rats with pulmonary hypertension. *Am J Physiol Heart Circ Physiol*. 2009;297:H1606–16.

21. Pietra GG, Capron F, Stewart S, Leone O, Humbert M, Robbins IM, et al. Pathologic assessment of vasculopathies in pulmonary hypertension. *J Am Coll Cardiol*. 2004;43:255–325.
22. Foster WS, Suen CM, Stewart DJ. Regenerative cell and tissue-based therapies for pulmonary arterial hypertension. *Can J Cardiol*. 2014;30:1350–60.
23. Kilkeny C, Browne WJ, Cuthill IC, Emerson M, Altman DG. Improving bioscience research reporting: the ARRIVE guidelines for reporting animal research. *PLoS Biol*. 2010;8:e1000412.
24. Dominici M, Le Blanc K, Mueller I, Slaper-Cortenbach I, Marini F, Krause D, et al. Minimal criteria for defining multipotent mesenchymal stromal cells. The International Society for Cellular Therapy position statement. *Cytotherapy*. 2006;8:315–7.
25. Nora CC, Camassola M, Bellagamba B, Ikuta N, Christoff AP, Meirelles Lda S, et al. Molecular analysis of the differentiation potential of murine mesenchymal stem cells from tissues of endodermal or mesodermal origin. *Stem Cells Dev*. 2012;21:1761–8.
26. Antunes MA, Abreu SC, Cruz FF, Teixeira AC, Lopes-Pacheco M, Bandeira E, et al. Effects of different mesenchymal stromal cell sources and delivery routes in experimental emphysema. *Respir Res*. 2014;15:118.
27. Thibault HB, Kurtz B, Raheer MJ, Shaik RS, Waxman A, Derumeaux G, et al. Noninvasive assessment of murine pulmonary arterial pressure: validation and application to models of pulmonary hypertension. *Circ Cardiovasc Imaging*. 2010;3:157–63.
28. Lang RM, Badano LP, Mor-Avi V, Afilalo J, Armstrong A, Ernande L, et al. Recommendations for cardiac chamber quantification by echocardiography in adults: an update from the American Society of Echocardiography and the European Association of Cardiovascular Imaging. *J Am Soc Echocardiogr*. 2015;28:1–39. e14.
29. Abreu SC, Antunes MA, de Castro JC, de Oliveira MV, Bandeira E, Omellas DS, et al. Bone marrow-derived mononuclear cells vs. mesenchymal stromal cells in experimental allergic asthma. *Respir Physiol Neurobiol*. 2013;187:190–8.
30. Russell Jr HK. A modification of Movat's pentachrome stain. *Arch Pathol*. 1972;94:187–91.
31. Spieth PM, Carvalho AR, Guldner A, Kasper M, Schubert R, Carvalho NC, et al. Pressure support improves oxygenation and lung protection compared to pressure-controlled ventilation and is further improved by random variation of pressure support. *Crit Care Med*. 2011;39:746–55.
32. Uhlig C, Silva PL, Ornellas D, Santos RS, Miranda PJ, Spieth PM, et al. The effects of salbutamol on epithelial ion channels depend on the etiology of acute respiratory distress syndrome but not the route of administration. *Respir Res*. 2014;15:56.
33. Weibel ER. Morphometry: stereological theory and practical methods. In: Gill J, editor. *Models of Lung Disease: Microscopy and Structural Methods*. New York: Dekker; 1990. p. 199–247.
34. Akamine R, Yamamoto T, Watanabe M, Yamazaki N, Kataoka M, Ishikawa M, et al. Usefulness of the 5' region of the cDNA encoding acidic ribosomal phosphoprotein P0 conserved among rats, mice, and humans as a standard probe for gene expression analysis in different tissues and animal species. *J Biochem Biophys Methods*. 2007;70:481–6.
35. Schmittgen TD, Livak KJ. Analyzing real-time PCR data by the comparative C(T) method. *Nat Protoc*. 2008;3:1101–8.
36. Larionov A, Krause A, Miller W. A standard curve based method for relative real time PCR data processing. *BMC Bioinformatics*. 2005;6:62.
37. Seluanov A, Vaidya A, Gorbunova V. Establishing primary adult fibroblast cultures from rodents. *J Vis Exp*. 2010;(44). doi:10.3791/2033.
38. Krzywinski M, Altman N. Points of significance: Comparing samples—part II. *Nat Methods*. 2014;11:355–6.
39. Nogueira-Ferreira R, Vitorino R, Ferreira R, Henriques-Coelho T. Exploring the monocrotaline animal model for the study of pulmonary arterial hypertension: a network approach. *Pulm Pharmacol Ther*. 2015;35:8–16.
40. Meyrick B, Gamble W, Reid L. Development of Crotalaria pulmonary hypertension: hemodynamic and structural study. *Am J Physiol*. 1980;239:H692–702.
41. Gomez-Arroyo JG, Farkas L, Alhussaini AA, Farkas D, Kraskauskas D, Voelkel NF, et al. The monocrotaline model of pulmonary hypertension in perspective. *Am J Physiol Lung Cell Mol Physiol*. 2012;302:L363–9.
42. Ricard N, Tu L, Le Hiress M, Huertas A, Phan C, Thuillet R, et al. Increased pericyte coverage mediated by endothelial-derived fibroblast growth factor-2 and interleukin-6 is a source of smooth muscle-like cells in pulmonary hypertension. *Circulation*. 2014;129:1586–97.
43. Dabral S, Tian X, Kojonazarov B, Savai R, Ghofrani HA, Weissmann N, et al. Notch1 signalling regulates endothelial proliferation and apoptosis in pulmonary arterial hypertension. *Eur Respir J*. 2016;48:1137–49.
44. McMurtry MS, Archer SL, Altieri DC, Bonnet S, Haromy A, Harry G, et al. Gene therapy targeting survivin selectively induces pulmonary vascular apoptosis and reverses pulmonary arterial hypertension. *J Clin Invest*. 2005;115:1479–91.
45. Jonigk D, Golpon H, Bockmeyer CL, Maegel L, Hoepfer MM, Gottlieb J, et al. Plexiform lesions in pulmonary arterial hypertension composition, architecture, and microenvironment. *Am J Pathol*. 2011;179:167.
46. Abdel-Kawi SH, Hashem KS. Possible therapeutic effect of stem cell in atherosclerosis in albino rats. A histological and immunohistochemical study. *Int J Stem Cells*. 2015;8:200–8.
47. Park KW, Yang HM, Youn SW, Yang HJ, Chae IH, Oh BH, et al. Constitutively active glycogen synthase kinase-3beta gene transfer sustains apoptosis, inhibits proliferation of vascular smooth muscle cells, and reduces neointima formation after balloon injury in rats. *Arterioscler Thromb Vasc Biol*. 2003;23:1364–9.
48. Gary-Bobo G, Houssaini A, Amsellem V, Rideau D, Pacaud P, Perrin A, et al. Effects of HIV protease inhibitors on progression of monocrotaline- and hypoxia-induced pulmonary hypertension in rats. *Circulation*. 2010;122:1937–47.
49. Orriols M, Gomez-Puerto MC, Ten Dijke P. BMP type II receptor as a therapeutic target in pulmonary arterial hypertension. *Cell Mol Life Sci*. 2017;74:2979–95.
50. McMurtry MS, Moudgil R, Hashimoto K, Bonnet S, Michelakis ED, Archer SL. Overexpression of human bone morphogenetic protein receptor 2 does not ameliorate monocrotaline pulmonary arterial hypertension. *Am J Physiol Lung Cell Mol Physiol*. 2007;292:L872–8.
51. Ranchoux B, Antigny F, Rucker-Martin C, Hautefort A, Pechoux C, Bogaard HJ, et al. Endothelial-to-mesenchymal transition in pulmonary hypertension. *Circulation*. 2015;131:1006–18.
52. Ohnishi S, Guntert P, Koshiba S, Tomizawa T, Akasaka R, Tochio N, et al. Solution structure of an atypical WW domain in a novel beta-clam-like dimeric form. *FEBS Lett*. 2007;581:462–8.
53. Wang M, Crisostomo PR, Herring C, Meldrum KK, Meldrum DR. Human progenitor cells from bone marrow or adipose tissue produce VEGF, HGF, and IGF-I in response to TNF by a p38 MAPK-dependent mechanism. *Am J Physiol Regul Integr Comp Physiol*. 2006;291:R880–4.
54. Ferrara N. Role of vascular endothelial growth factor in regulation of physiological angiogenesis. *Am J Physiol Cell Physiol*. 2001;280:C1358–66.
55. Tudor RM, Chacon M, Alger L, Wang J, Taraseviciene-Stewart L, Kasahara Y, et al. Expression of angiogenesis-related molecules in plexiform lesions in severe pulmonary hypertension: evidence for a process of disordered angiogenesis. *J Pathol*. 2001;195:367–74.
56. Nam HS, Kwon I, Lee BH, Kim H, Kim J, An S, et al. Effects of mesenchymal stem cell treatment on the expression of matrix metalloproteinases and angiogenesis during ischemic stroke recovery. *PLoS One*. 2015;10:e0144218.
57. Bortolotti F, Ukovich L, Razban V, Martinelli V, Ruozi G, Pelos B, et al. In vivo therapeutic potential of mesenchymal stromal cells depends on the source and the isolation procedure. *Stem Cell Reports*. 2015;4:332–9.
58. Diaz-Flores L, Gutierrez R, Madrid JF, Varela H, Valladares F, Acosta E, et al. Pericytes. Morphofunction, interactions and pathology in a quiescent and activated mesenchymal cell niche. *Histol Histopathol*. 2009;24:909–69.
59. Waterman RS, Tomchuck SL, Henkle SL, Betancourt AM. A new mesenchymal stem cell (MSC) paradigm: polarization into a pro-inflammatory MSC1 or an immunosuppressive MSC2 phenotype. *PLoS One*. 2010;5:e10088.
60. Hansmann G, Fernandez-Gonzalez A, Aslam M, Vitali SH, Martin T, Mitsialis SA, et al. Mesenchymal stem cell-mediated reversal of bronchopulmonary dysplasia and associated pulmonary hypertension. *Pulm Circ*. 2012;2:170–81.
61. Rajashekhar G, Traktuev DO, Roell WC, Johnstone BH, Merfeld-Claus S, Van Natta B, et al. IFATS collection: Adipose stromal cell differentiation is reduced by endothelial cell contact and paracrine communication: role of canonical Wnt signaling. *Stem Cells*. 2008;26:2674–81.
62. Chen JY, An R, Liu ZJ, Wang JJ, Chen SZ, Hong MM, et al. Therapeutic effects of mesenchymal stem cell-derived microvesicles on pulmonary arterial hypertension in rats. *Acta Pharmacol Sin*. 2014;35:1121–8.
63. Lee C, Mitsialis SA, Aslam M, Vitali SH, Vergadi E, Konstantinou G, et al. Exosomes mediate the cytoprotective action of mesenchymal stromal cells on hypoxia-induced pulmonary hypertension. *Circulation*. 2012;126:2601–11.
64. Sakao S, Taraseviciene-Stewart L, Wood K, Cool CD, Voelkel NF. Apoptosis of pulmonary microvascular endothelial cells stimulates vascular smooth muscle cell growth. *Am J Physiol Lung Cell Mol Physiol*. 2006;291:L362–8.

65. Alencar AK, Pereira SL, Montagnoli TL, Maia RC, Kummerle AE, Landgraf SS, et al. Beneficial effects of a novel agonist of the adenosine A2A receptor on monocrotaline-induced pulmonary hypertension in rats. *Br J Pharmacol*. 2013;169:953–62.
66. Alencar AK, Pereira SL, da Silva FE, Mendes LV, Cunha Vdo M, Lima LM, et al. N-acylhydrazone derivative ameliorates monocrotaline-induced pulmonary hypertension through the modulation of adenosine AA2R activity. *Int J Cardiol*. 2014;173:154–62.
67. Abbas AE, Franey LM, Marwick T, Maeder MT, Kaye DM, Vlahos AP, et al. Noninvasive assessment of pulmonary vascular resistance by Doppler echocardiography. *J Am Soc Echocardiogr*. 2013;26:1170–7.
68. Granstam SO, Bjorklund E, Wikstrom G, Roos MW. Use of echocardiographic pulmonary acceleration time and estimated vascular resistance for the evaluation of possible pulmonary hypertension. *Cardiovasc Ultrasound*. 2013;11:7.
69. Maarman G, Lecour S, Butrous G, Thienemann F, Sliwa K. A comprehensive review: the evolution of animal models in pulmonary hypertension research; are we there yet? *Pulm Circ*. 2013;3:739–56.
70. Morty RE, Nejman B, Kwapiszewska G, Hecker M, Zakrzewicz A, Kouri FM, et al. Dysregulated bone morphogenetic protein signaling in monocrotaline-induced pulmonary arterial hypertension. *Arterioscler Thromb Vasc Biol*. 2007;27:1072–8.
71. Arcot SS, Lipke DW, Gillespie MN, Olson JW. Alterations of growth factor transcripts in rat lungs during development of monocrotaline-induced pulmonary hypertension. *Biochem Pharmacol*. 1993;46:1086–91.
72. Ferrara N, Gerber HP, LeCouter J. The biology of VEGF and its receptors. *Nat Med*. 2003;9:669–76.

Submit your next manuscript to BioMed Central and we will help you at every step:

- We accept pre-submission inquiries
- Our selector tool helps you to find the most relevant journal
- We provide round the clock customer support
- Convenient online submission
- Thorough peer review
- Inclusion in PubMed and all major indexing services
- Maximum visibility for your research

Submit your manuscript at
www.biomedcentral.com/submit

